Proc. Indian Acad. Sci. (*Chem. Sci.*), Vol. 113, Nos 5 & 6, October–December 2001, pp 633–649

Synthesis and properties of $MoSi_2$ based engineering ceramics

P SRIKARI TANTRI, ANUP K BHATTACHARYA and
SHEELA K RAMASESHA*
National Aerospace Laboratories (NAL), Bangalore 560 017, India
e-mail: sheela@css.cmmacs.ernet.in

Abstract. Molybdenum disilicide is a high temperature structural ceramic with many attractive properties for engineering applications. Foremost amongst these is its stability in corrosive atmospheres up to about 1600°C. However, there are a few undesirable properties that need to be addressed before it can become a viable material in high temperature applications. Since $MoSi_2$ forms thermodynamically stable composites with both metals and ceramics, many reinforcing materials are incorporated into the matrix to improve the fracture toughness and creep properties. The low temperature oxidation can be controlled by making high density (> 95% of theoretical density) compacts. This article summarizes the important attempts that are made in improving the properties of molybdenum disilicide-based ceramics by the reinforcement with other materials.

Keywords. Molybdenum disilicide; high temperature applications; reactive infiltration.

1. Introduction

Because of the progress in technology, the demand on materials that can withstand high temperatures for long duration of time and tolerate high stresses in aggressive environments has increased. The two critical requirements that must be satisfied in order for a structural material to be successfully used in elevated temperature applications are high oxidation resistance to prevent degradation during high temperature exposure and attractive combination of mechanical properties. Of the structural ceramics silicides and aluminides have become important because of their corrosion resistance at high temperatures. The intermetallic compound $MoSi_2$ (having weak metallic bonding between Mo–Mo atoms and Mo–Si strong covalent bonds) has many attractive properties like high melting temperature (2030°C) and moderate density of 6·3 g/cm^3. It has high oxidation resistance at high temperatures in corrosive atmospheres. Other important and useful properties of $MoSi_2$ are:

- It undergoes a brittle-to-ductile transition (BDTT) around 1000°C and thus exhibiting plasticity above this temperature [1]. Because of this ductility at high temperatures the components made out of $MoSi_2$ will not undergo catastrophic failure.
- It has a high Young's modulus of 440 GPa [2].
- It is a good thermal conductor [3].
- It can form thermodynamically stable alloys and composites with other ceramics and metals unlike many high temperature structural ceramics including SiC [4].

*For correspondence

- It has better chemical resistance towards hot corrosion by NaCl, V_2O_5 and H_2S than best superalloys [5].
- It can be machined by electrodischarge machining because of its high electrical conductivity.

However, $MoSi_2$ has a few undesirable properties like 'PEST'ing [6], low fracture toughness at low temperatures and low creep resistance at high temperatures [7].

Before $MoSi_2$ related materials could be used for structural applications in high performance engines the above shortcomings need to be addressed. Many brittle (like SiC, TiB_2, Si_3N_4 etc.) and ductile (like Nb, Ta, W, Al) reinforcements, in particulate, whisker and fibre form, have been attempted to improve the mechanical strength of $MoSi_2$. Fracture toughness of $MoSi_2$ is in the range of 2·6 to 5·1 $MPam^{1/2}$ at room temperature [8,9]. Fracture toughness is found to increase with decrease in grain size [10]. By reinforcing it with Nb fibres the fracture toughness has been increased to values as high as 15 $MPam^{1/2}$ [11–13]. The toughness of the SiC composite is found to be a function of volume fraction of SiC [14–16]. In the SiC particulate reinforcement maximum toughness is obtained with 20 vol% SiC. The reinforcement of partially stabilized zirconia (PSZ) into $MoSi_2$ matrix is found to improve the mechanical properties of $MoSi_2$ due to its low temperature transformation toughening [17]. The increase in the toughness with SiC and ZrO_2 double reinforcement was greater than that with ZrO_2 alone. The fracture strength is found to be maximum (~1050 MPa) with reinforcement of >15 mol% 3Y–ZrO_2 and the fracture toughness improves to about 4·5 $MPam^{1/2}$.

Beyond BDTT, $MoSi_2$ undergoes plastic deformation and creep deformation increases with increasing temperature. Also presence of silica at grain boundaries enhances deformation at high temperatures. Reinforcement of Mo, W, C and SiC significantly improves creep resistance of $MoSi_2$ [18]. Creep of SiC–$MoSi_2$ composites have been widely studied with SiC particulates and whiskers. Creep rate in monolithic $MoSi_2$ is found to be around 10^{-6} to 10^{-4} s^{-1} for stresses up to 10^3 MPa. The addition of 40 vol% SiC decreases the creep rate to about 10^{-8} s^{-1} for the same stress ranges [19]. SiC whisker reinforcement improves creep properties further as found in $MoSi_2$ – WSi_2 with 20 vol% SiC(*w*) where the creep rate is 10^{-9} to 10^{-7} s^{-1} [20].

$MoSi_2$ is found to be extremely wear resistant in a severe two-body abrasive environment [21–23]. It is an attractive wear resistant material for application in high temperature corrosive and oxidative environment because of its high hardness, high elastic modulus and good oxidation resistance at elevated temperatures.

Many workers have been investigating aluminum reinforcement into $MoSi_2$ matrix. Fracture toughness increases with increase in aluminum content in the matrix. This is attributed to the formation of a more ductile $Mo(Al,Si)_2$ phase with C40 structure. Mitra *et al* [24] have varied the Al content from 1·5 to 5 wt% in $MoSi_2$ matrix and found that Al reduced SiO_2 content in $MoSi_2$ by forming Al_2O_3. The surplus Al reacted with $MoSi_2$ to form $Mo(Al,Si)_2$. Hence the compacts with high Al content has three phases, namely, $MoSi_2$, $Mo(Al,Si)_2$ and α– Al_2O_3. The fracture toughness increases to 6·4 $MPam^{1/2}$ in 5 wt% Al.

In this article we have briefly summarized our attempts at improving the properties of $MoSi_2$ and $Mo(Al,Si)_2$ systems. We have synthesized both ductile and brittle reinforced composites. We have studied various physical, chemical and mechanical properties. In §2, we discuss the properties of $MoSi_2$ and its composites. In §3, we discuss the studies of $Mo(Al,Si)_2$ and its composites.

2. $MoSi_2$ and its composites

The reaction between Mo and Si is exothermic with a ΔH of –36 kcal/mol. Hence $MoSi_2$ can be synthesized by the SHS (Self-propagating high temperature synthesis) route. The product is usually highly porous. In order to obtain a fully dense $MoSi_2$ compact in a single step, the product must be hot-pressed as it is forming. For this purpose we have assembled a temperature controlled induction heated hot-pressing apparatus (figure 1). Here a stoichiometric mixture of elemental Mo and Si is hot pressed at 1800°C under a pressure of 20 MPa. By varying the temperature and pressure the density of the compact can be controlled. To make the composites particulates of TiB_2 and SiC in required proportion are ball milled with Mo and Si powders. This mixture is hot pressed to get the composite compacts.

2.1 *'PEST'ing*

$MoSi_2$ reacts with oxygen when heated in air to form MoO_3 and SiO_2. At temperatures higher than 750°C, MoO_3 volatilizes leaving behind a layer of SiO_2 on the surface of $MoSi_2$ that effectively prevents diffusion of oxygen thereby spares the oxidation of $MoSi_2$ in the interior. However, at low temperatures, below 700°C, MoO_3 does not volatilize and the oxide layer is highly porous, providing an easy passage for oxygen diffusion. This could in some cases result in oxidation accompanied by complete disintegration of the compact into powdery products, which is termed 'pest'ing. Controlling pesting has been the topic of many investigations [6,25,26]. Pesting is reportedly most prominent at 500°C in air. It is found also that controlling defects like pores, microcracks and intergranular boundaries reduces pesting to a large extent as pesting has been attributed to the accelerated formation of voluminous MoO_3 in microcracks. Hence pesting should not occur in a dense compact of $MoSi_2$. However, there are reports to the contrary [27]. Chou and Nieh [28], from their experiments on $MoSi_2$–AlN and $MoSi_2$–Al_2O_3 composites have found that foreign additives have an effect on the kinetics of the pest disintegration. On the other hand, $MoSi_2$ + 20 vol% SiC compacts prepared by hot pressing and with high

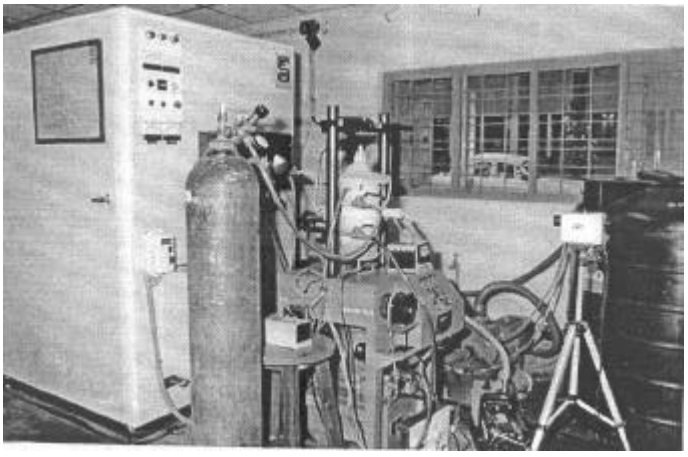

Figure 1. The induction heated temperature controlled hot-press.

density do not show disintegration even after heating for 250 h at 500°C, though the regions close to interfaces and grain boundaries are oxidized preferentially.

In order to understand whether it is the density or the inclusion that has prominent effect on 'pest'ing in $MoSi_2$ we have synthesized high density compacts with deliberate inclusion of foreign phases like Mo_5Si_3, SiC and Mo_5Si_3C in addition to SiO_2 (which is always present in $MoSi_2$). Rectangular samples cut from the compacts, polished with 1 μm diamond paste and pesting experiments were carried out on these samples at 500°C for 100 h[29]. None of the samples disintegrated even after 100 h of heating. Samples were fractured to see the changes that might have taken place in the bulk. SEM of samples after oxidation test is shown in figure 2. There was no visible change on either the polished or the fractured surface of monolithic $MoSi_2$. $Mo(Al,Si)_2$ surface had many open blisters containing rod like MoO_3 in them and the surface of the blister was still $Mo(Al,Si)_2$ implying that there is no oxidation of $Mo(Al,Si)_2$ confirming the observation of Maruyama and Yanagihara[30]. Mo_5Si_3 that was present before heating was no longer present in the oxidized samples. It seems likely that the Mo_5Si_3 is preferentially oxidized as Mo_5Si_3 has poor oxidation resistance than $MoSi_2$. The oxidation of Mo_5Si_3 proceeds as,

$$2Mo_5Si_3 + 21\,O_2 \rightarrow 10MoO_3 + 6\,SiO_2, \quad (1)$$

and the change in volume may be responsible for the formation and opening up of the blisters. No such blisters were observed in $MoSi_2$ + 1 wt% C which had only MoO_3 whiskers and SiO_2 on the surface. It is possible that the passage of oxygen through Mo_5Si_3C is more difficult than through Mo_5Si_3 preventing formation of blisters. Mo_5Si_3C reacts with oxygen to form MoO_3, SiO_2 and CO_2. MoO_3 and SiO_2 are seen on the surface of the oxidized sample.

The SEM of the fractured surface in all the above samples did not show any indication of oxidation inside the body. Even in the severely oxidized $Mo(Al,Si)_2$ and $MoSi_2$ + 1%C samples the oxidation is superficial and the oxidation has not penetrated deeper into the compact. The high density of the compacts prevents the oxygen from diffusing into the compact and thereby leading to disintegration of the compact even though there were small amounts of impurities. The pesting requires oxide propagation through pores and cracks and grain boundary oxidation is only marginal[31]. Thus, pesting in $MoSi_2$ containing impurities could be controlled with the full densification of the compact in the absence of external stress.

2.2 *Mechanical properties*

Hardness of the compacts is found to increase with increase in density. The 86% dense monolith has low hardness of 8·8 GPa and that of 99% is 9·8 GPa. The addition of 10 and 20 wt% TiB_2 was found to increase the hardness to 10·2 and 11·2 GPa, respectively[32].

Wear resistance experiments were carried out on a pin-on-disc apparatus. Variation of the specific wear rate with normal load for monoliths of different densities and 20% TiB_2 composite is shown in figure 3. The specific wear rate decreases with increasing load (non steady state) at lower loads and remains almost constant over a certain load range (mild wear region) before increasing beyond an upper critical load (severe wear region). It is seen that wear rate decreases with increase in density of the monolith. Figure 4 gives lower and the upper critical loads of the mild wear regime for monoliths of different

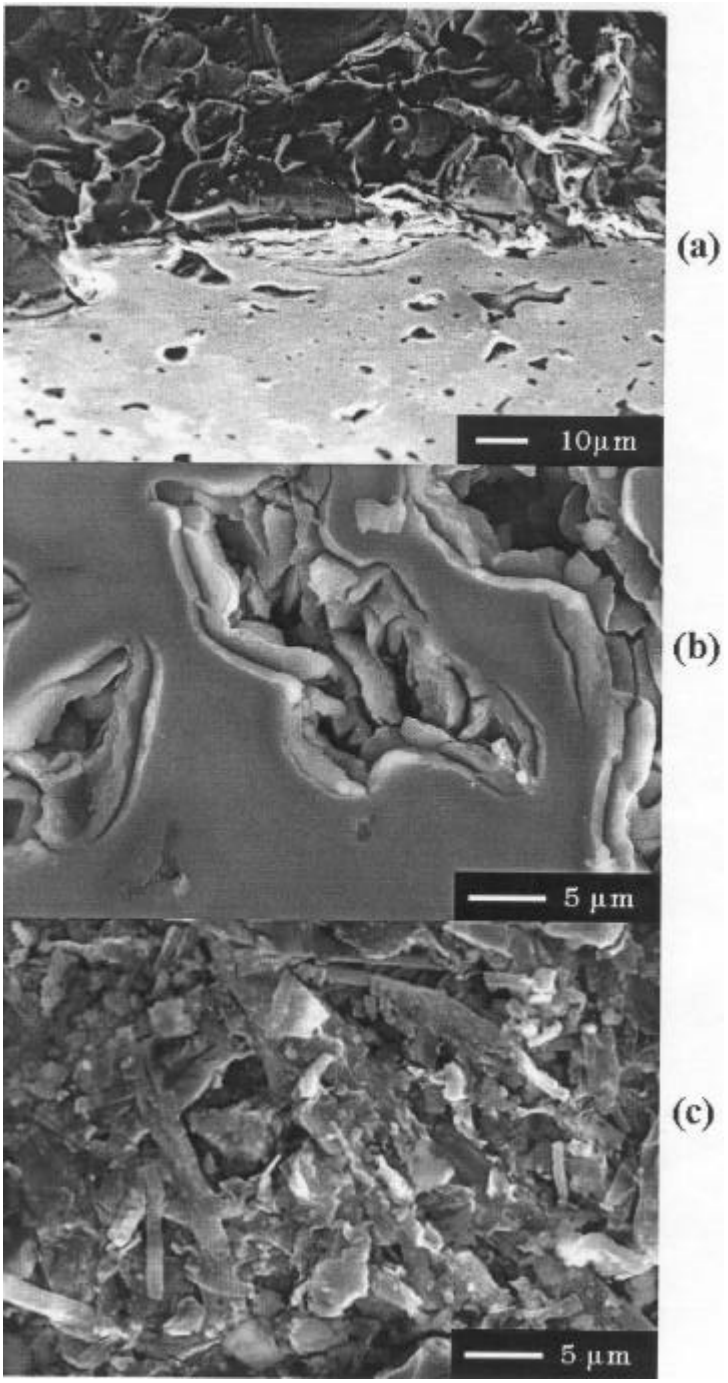

Figure 2. SEM of the samples after the oxidation experiment. (**a**) $MoSi_2$, at the edge of the fractured surface. No visible oxidation on either surface; (**b**) the open blisters on the surface of $Mo(Al,Si)_2$. MoO_3 rods are seen inside the open blisters; (**c**) MoO_3 rods are seen on the surface of $MoSi_2$ + 1 wt% C.

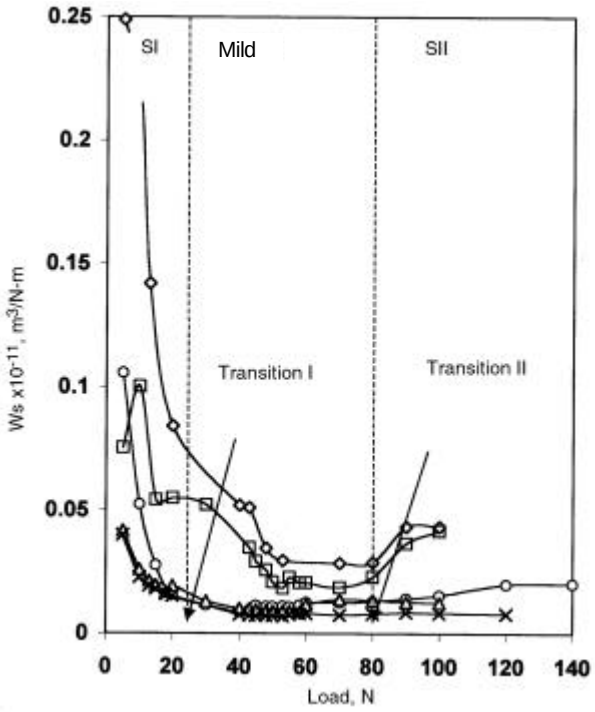

Figure 3. Specific wear rate (*Ws*) vs load (*N*) for monoliths of different densities and the composite. [–◇– 86%, –□– 93%, –○– 98% and composites (–×– 10% and –Δ– 20% TiB_2)]. Regions SI and SII refer to the first and second severe wear regimes with mild wear in between them.

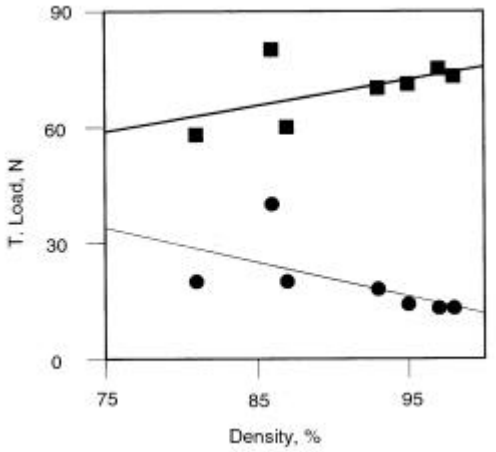

Figure 4. Variation of upper (■) and lower (●) transition loads as a function of the density for the monolithic $MoSi_2$.

densities. The lower critical load decreases whereas the upper critical load increases with increase in density of the pin. The difference between the two critical loads, signifying

the load spans of mild wear regime, increases with increasing density of the pin[33]. It is observed that at a given load coefficient of friction (COF) decreases with increase in density. The COF of reinforced samples is less than that of the monolith.

At the end of sliding experiment, a dark brown film adhering firmly on to the pin surface is observed for all the samples. The X-ray mapping (as shown in figures 5a and b) of the film revealed the presence of elements of the disc material like Fe, Ni and Cr[34]. Oxygen content is also very high. During sliding, the debris formed at the initial loads are entrapped in the depressions and the grooves of the disc surface getting compacted. The relative motion of the rubbing surfaces leads to tearing of the asperities in the disc material, which leads to the transfer of the disc material to pin. The disc material may get oxidized after being transferred to the pin. Thus a layer of either transferred metal or

(a)

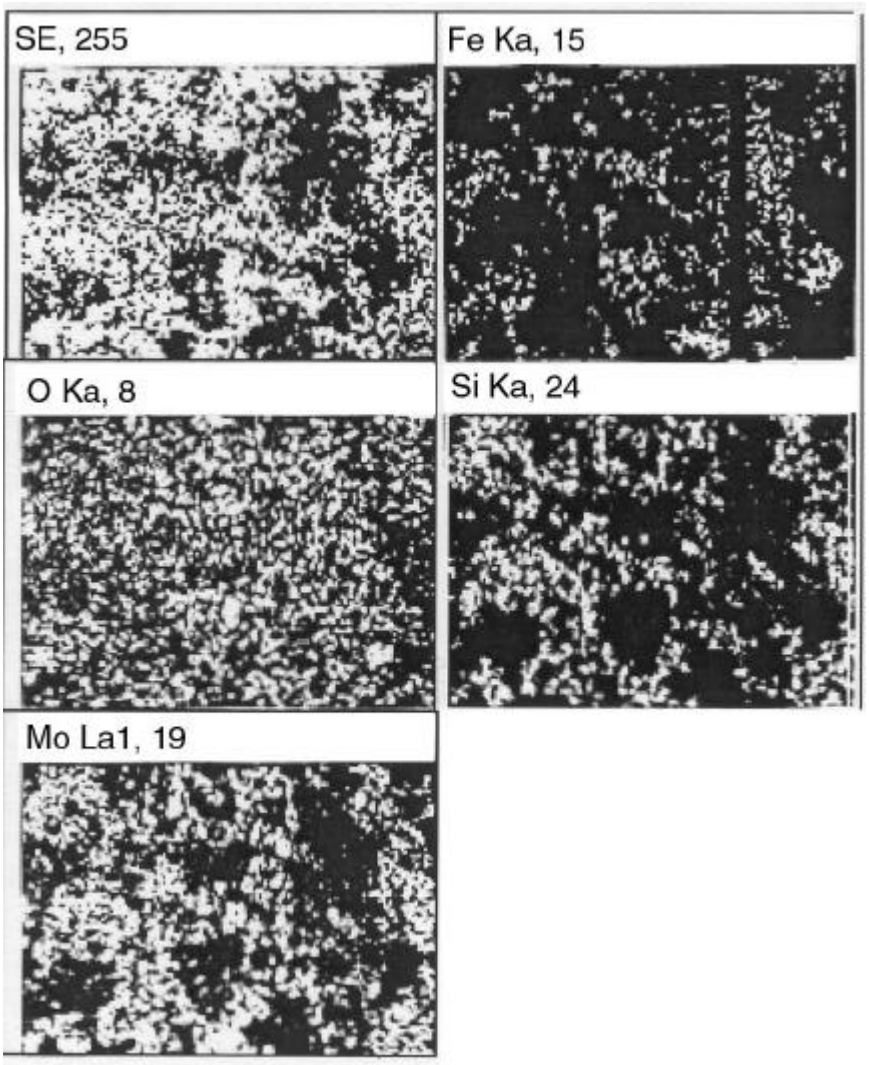

Figure 5. (**a**) (Caption on the next page.)

(b)

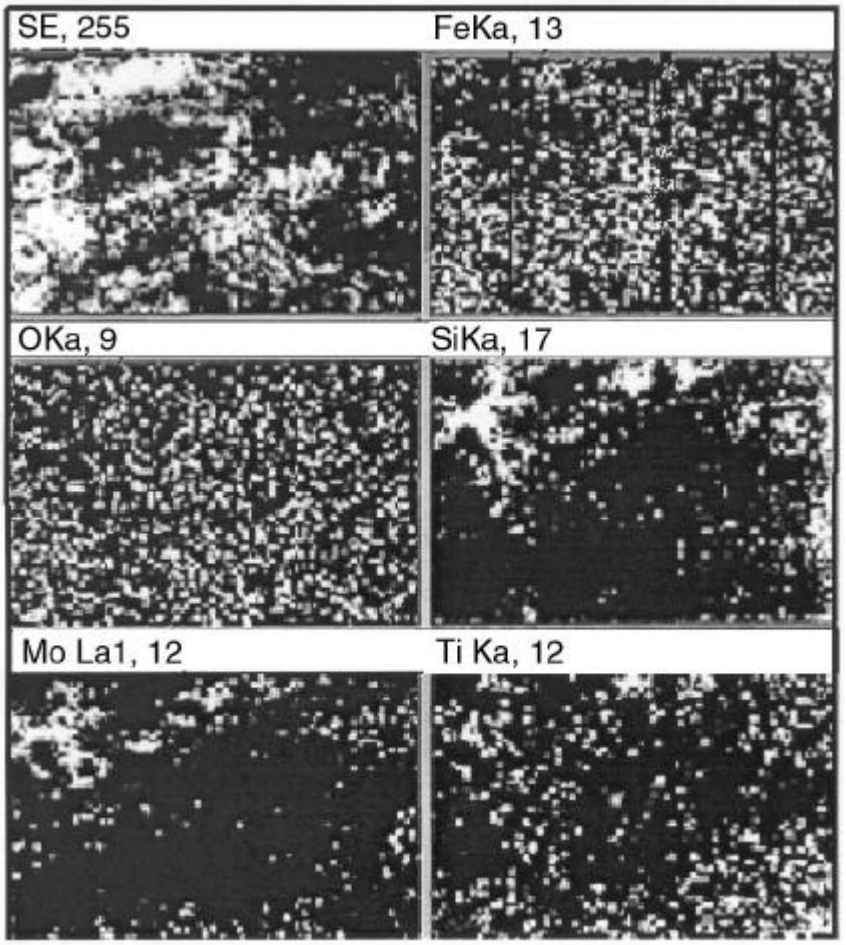

Figure 5. X-ray mapping of the monolithic (**a**) and 20% TiB_2 composite (**b**) pins, after the wear experiments.

compacted oxides is continuously formed during the sliding between the pin and the disc. As the film starts forming the pin enters the mild wear regime and the sliding is between the film and the disc resulting in less wear of the pin. At loads greater than the upper critical loads, the stability of the film may be lost as the subsurface undergoes plastic deformation and the pin enters the severe wear region.

The surface temperatures of the monolithic as well as the composite pins were calculated as a function of time using a one-dimensional heat transfer equation in the three regions, i.e. SI, mild and SII and are shown in figure 6. The surface temperatures were higher for lower density compacts as pores are bad conductors of heat. In the SI region the surface temperatures are in the range of 90–200°C. The levels of temperature at 50 N load roughly correspond to the level of the friction force. For monoliths of density less than 98% the mild wear regime ends at 75 N. For the highly dense monolith and $MoSi_2 + TiB_2$ composites that are less dense (93%), the mild wear regime extends to 140 N. From figure 6 the estimated interface temperature is in the range 500–600°C. It is

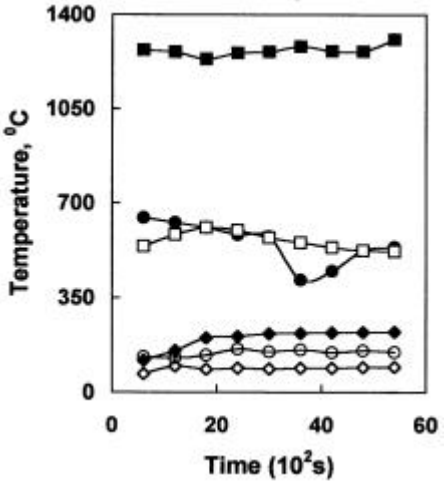

Figure 6. Variation of estimated temperature with time. Diamonds: 15 N, circles: 50 N, squares: 75 N for monolith of 93% density (filled symbols) and 20% TiB_2+$MoSi_2$ composite (open symbols): Speed = 0·5 m/s.

possible that both TiB_2 and $MoSi_2$ oxidize at these temperatures yielding a borosilicate glass. These interfacial temperatures are not far away from the softening temperature of such a glass and the disc/pin interface may be layered with a semi-viscous borosilicate. This would promote easy shear, low friction and thus low wear. In the SII region the surface temperature for the 93% density monolith reaches as high as 1300°C. As the temperature increases, the viscosity of the glassy film decreases and its lubrication properties diminish. As the severity of sliding is increased, the wear surfaces become rough due to high friction and wear and the pins enter the severe wear regime [35].

After the wear experiments, the $MoSi_2$–TiB_2 composite pin surface did not show the presence of TiB_2 particles. The TiB_2–SiC double reinforced $MoSi_2$ pins contained only SiC particles (figure 7). It seems that TiB_2 decomposes because of the friction and wear. Detailed analysis of the tribofilm is currently in progress.

The room temperature flexural strength of monolithic $MoSi_2$ is about 150 MPa. With 10% TiB_2 reinforcement it has increased to 400 MPa. However, the flexural strength of double reinforced composite increases to only 240 MPa. High temperature fracture toughness and bending strength studies are currently being carried out.

3. $Mo(Al,Si)_2$ and its composites

$Mo(Al_xSi_{1-x})_2$ [$Mo(Al_xSi_{1-x})_2$ (designated as MAS) has been synthesized by hot-pressing the elements in required proportion for $x = 0{\cdot}5$ [36]. Hot-pressing is carried out at different temperatures. It is found that single phase MAS, in the absence of excess Al, is formed in the temperature range of 1300 to 1400°C. The sample synthesized at 1500°C contained many impurity lines of Mo_5Si_3 in the X-ray diffraction pattern. The SEM of the sample synthesized at 1300°C shows single particle type. The mechanical properties for structural applications are currently under study.

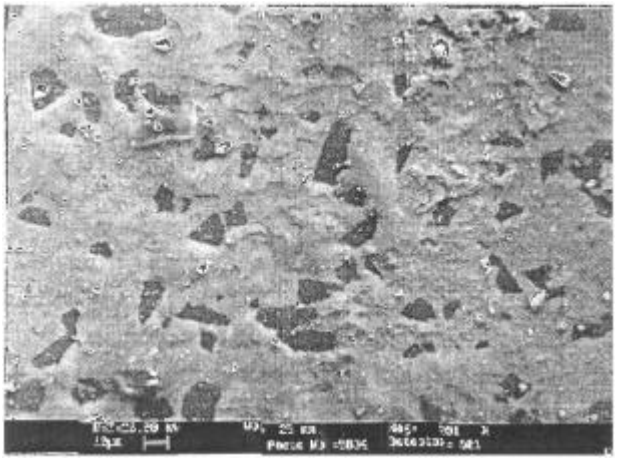

Figure 7. SEM of the SiC + TiB_2 double reinforced pin surface after wear experiment. SiC particles are observed but TiB_2 particulates are not.

Obtaining high purity MAS and its composites is difficult by conventional methods, here an alternative method of synthesis, known as melt infiltration [37] is attempted. Melt infiltration is a versatile and cost effective method of preparing ceramic–metal composites. In this method, the metal, which has lower melting temperature than the ceramic, melts upon heating and penetrates into the porous ceramic preform. With this technique it is possible, not only to obtain a near net-shaped component but also a product with low residual porosity. If during infiltration the melt reacts with the preform to form a new compound, the process is called reactive melt infiltration (RMI). Experimental conditions such as the atmosphere in which infiltration is carried out and the temperature affect the rate of infiltration [38].

Infiltration process may be explained by a capillary rise and viscous flow mechanisms [39]. For example, activation energy of 8·4 kJ/mol has been found for the infiltration of lead into copper powder compact [40]. This value is very close to the activation energies for viscous flow and self-diffusion of liquid lead. But there are some infiltration processes where activation energy value is quite large compared to the activation energy of viscous flow of the infiltrant metal. Activation energies of 92 and 67 kJ/mol were found for the infiltration of liquid lead and indium into porous titanium powder compacts respectively [41], which are an order of magnitude larger than the activation energies for viscous flow of molten lead and indium. So it was concluded that some chemical reaction is controlling the infiltration rate. It is well known that physical processes such as viscous flow of simple liquids or physical adsorption usually require an activation energy less than 80 kJ/mol while chemical processes such as vaporization, chemisorption or solid state reactions require much higher activation energies. We have studied the infiltration mechanism of aluminum into molybdenum silicide preform and the results are presented here.

3.1 *RMI into $MoSi_2$*

$MoSi_2$ pellets (40 and 85% dense) were made by cold- and hot-pressing the $MoSi_2$ powder respectively. Infiltration was carried out by placing Al–Si alloy atop these pellets.

Infiltration temperature was varied from 1050 to 1250°C and infiltration time from 5 to 30 min. Infiltration was carried out in argon atmosphere. After infiltration, samples were cut and the cross-section was polished on 1 μ diamond paste to determine the microstructure and extent of infiltration.

RMI of Al into $MoSi_2$ preform proceeds as[36],

$$MoSi_2 + xAl \rightarrow Mo(Al_xSi_{1-x})_2 + 2xSi, \quad (2)$$

resulting in a $Mo(Al_xSi_{1-x})_2$ + Al + Si composite. This infiltration was successfully done with low as well as high-density preforms. Rate of infiltration was low at 1050°C but it increased drastically above 1100°C. Irrespective of the infiltration temperature and the preform density the MAS in the final product always contained 14–18 at% Al. Activation energy for the process was about 300 kJ/mol.

According to (2) when aluminum reacts with $MoSi_2$ some silicon gets replaced. This silicon is undesirable in the composite since it forms a eutectic with Al, which in turn degrades the properties of the composite. To absorb the by-product Si, a preform of a mixture of elemental Mo and $MoSi_2$ was used and the final composition after infiltration was found to contain no free silicon[42].

In an attempt to reduce the Al content in the final composite, a $MoSi_2$–Mo mixture was hot pressed at 1500°C to get a 85% dense preform. After sintering, the preform was found to contain $MoSi_2$ and Mo_5Si_3. SEM micrograph of this sample (figure 8) shows the presence of $MoSi_2$ (darker grey) and Mo_5Si_3 (lighter grey). Upon infiltration, this sample was found to contain MAS and Al–Si alloy. In the SEM micrograph of the sample (figure 9) the hexagonal grey coloured grains are MAS and the black area represents the Al–Si alloy. The rate of infiltration was much lower in the mixture preform; in a 2·5 mm thick sintered $MoSi_2$ + Mo sample even though the infiltration was first done at 1200°C for 15 min and then kept at 1600°C for 10 min, the infiltration was incomplete, whereas in 85% dense $MoSi_2$ preform of the same thickness infiltration was complete in 20 min at 1200°C. Hence, it could be the presence of Mo_5Si_3 in the initial preform that retards the rate. To understand this effect of Mo_5Si_3 on the rate, we have carried out RMI into pure Mo_5Si_3 preforms.

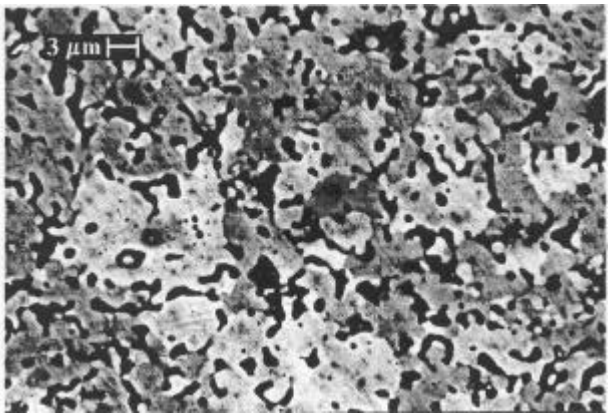

Figure 8. SEM micrograph of the sintered $MoSi_2$ + Mo preform. Darker grey portions are $MoSi_2$ while the lighter grey particles are Mo_5Si_3.

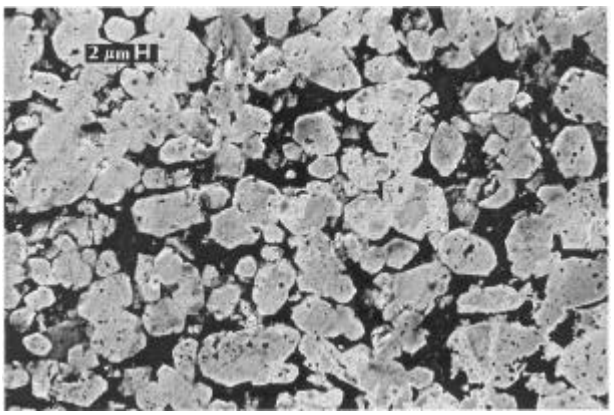

Figure 9. SEM micrograph of infiltrated $MoSi_2$ + Mo preform. The grey coloured grains are MAS and the black area is the Al–Si alloy.

3.2 *RMI into Mo_5Si_3*

Mo_5Si_3 was synthesized by mixing Mo and Si powders in stoichiometric proportion. The powder mixture was hot pressed in a graphite die at 1600°C at 10 MPa pressure to obtain almost 80% dense and 6 MPa pressure for a 60% dense Mo_5Si_3 sample. Hot pressed samples were then cut into four equal sized ($\sim 4{\cdot}8 \times \sim 3{\cdot}5 \times \sim 3{\cdot}5\ mm^3$) rectangular bars. Small aluminium – silicon alloy cubes were kept over these bars. The infiltration temperature was varied from 1200 to 1500°C keeping the duration constant at 20 min. In another set of experiments duration of infiltration was varied from 20 to 60 min. keeping the temperature constant at 1400°C. Infiltrated samples were cut and the cross section was well polished to study the infiltration process.

Infiltration in pure Mo_5Si_3 preform also resulted in MAS composite[43], microstructure of the infiltrated Mo_5Si_3 at 1400°C for 20 min is shown in figure 10. The infiltrated, uninfiltrated and the interface zone between them are seen. The black region is aluminum alloy and the dark grey region is found to contain aluminum (~74 at%), molybdenum (~21 at%) and silicon. Lighter grey hexagonal particles are MAS. On an average 25–27 at% of the aluminum is present in these MAS grains whereas 14 to 18 at% aluminum is present in the MAS grains after the infiltration of $MoSi_2$ preform. Thus the composition of the MAS formed after the infiltration depends on the chemical composition of the preform.

Even in the infiltrated Mo_5Si_3 at 1200°C, hexagonal grains are seen whereas in infiltrated $MoSi_2$ and $MoSi_2$ + Mo preform there is no clear grain morphology at this temperature. The grains are seen in these preforms only upon sintering at 1600°C after infiltration at 1200°C. This change in grain formation temperature may be due to the different Al content in the MAS grains. Al content in the MAS grains that are formed upon infiltrating Mo_5Si_3 preform is higher which could be leading to the lowering of recrystallization temperatures. Mo_5Si_3 samples infiltrated at 1400°C, for higher duration ($\geq$ 30 min) show well-developed hexagonal crystal like structures of MAS as seen in figure 11. The chemical composition of these structures was the same as that of the light grey hexagonal particles seen in figure 10.

Mo_5Si_3 reacts with aluminum as follows:

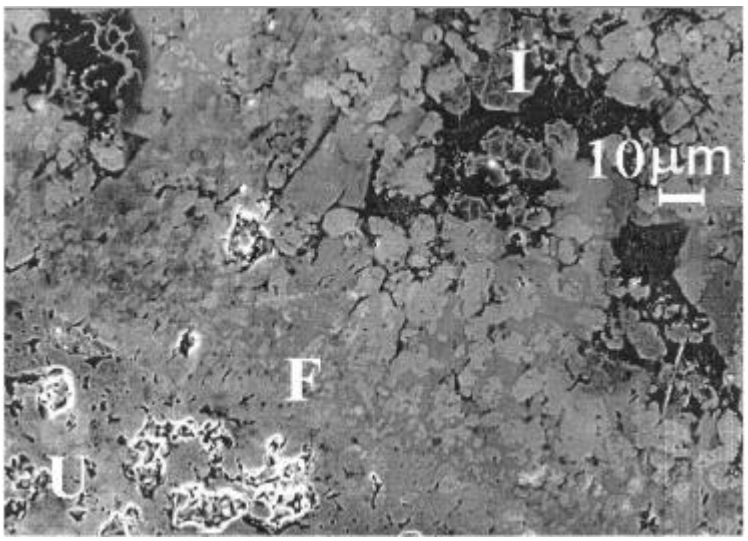

Figure 10. SEM of the infiltrated Mo_5Si_3 at 1400°C for 20 min showing the infiltrated (I), uninfiltrated (U) and the interface (F) zones.

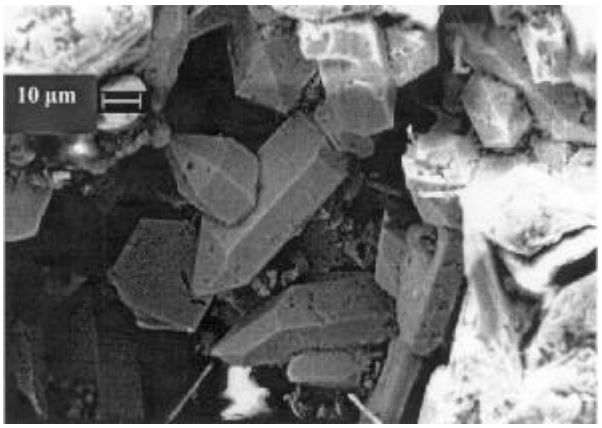

Figure 11. SEM of the fractured surface of Mo_5Si_3 infiltrated at 1400°C for 30 min, well-developed hexagonal crystal like structures of MAS are seen.

$$Mo_5Si_3 + 2x\ Al \rightarrow Mo(Al_xSi_{1-x})_2 + 4\ Mo + (1 + 2x)\ Si. \quad (3)$$

Elemental Mo that is released after the reaction diffuses in a direction opposite to infiltration direction. This reacts with the aluminum to form an Mo–Al phase. This phase is represented by dark grey region in figure 10. Well-developed and stacked parallelopiped crystals of this Mo–Al alloy are seen in a fractured surface of Mo_5Si_3 sample infiltrated at 1400°C for 30 min (figure 12). It is seen in figure 10 that this dark grey Mo–Al phase is mainly present near the infiltration front. Even the X-ray mapping (figure 13) shows that Mo is dense at the interface. Mo_5Si_3 sample infiltrated at temperatures higher than 1500°C has no individual grains, which may be because of the occurrence of excessive grain growth.

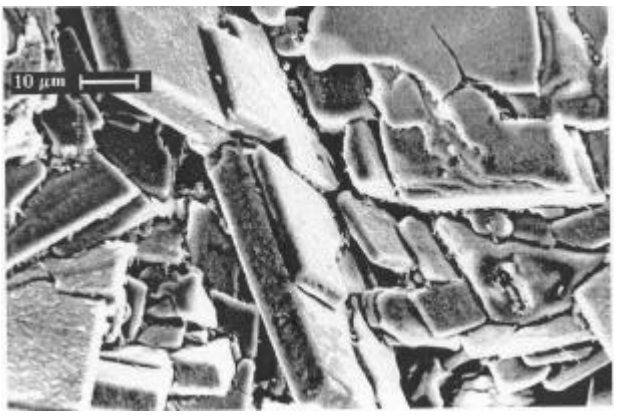

Figure 12. SEM micrograph of a fractured surface of the sample infiltrated at 1400°C for 30 min, well-developed and stacked parallelopiped structures of Mo–Al alloy are seen.

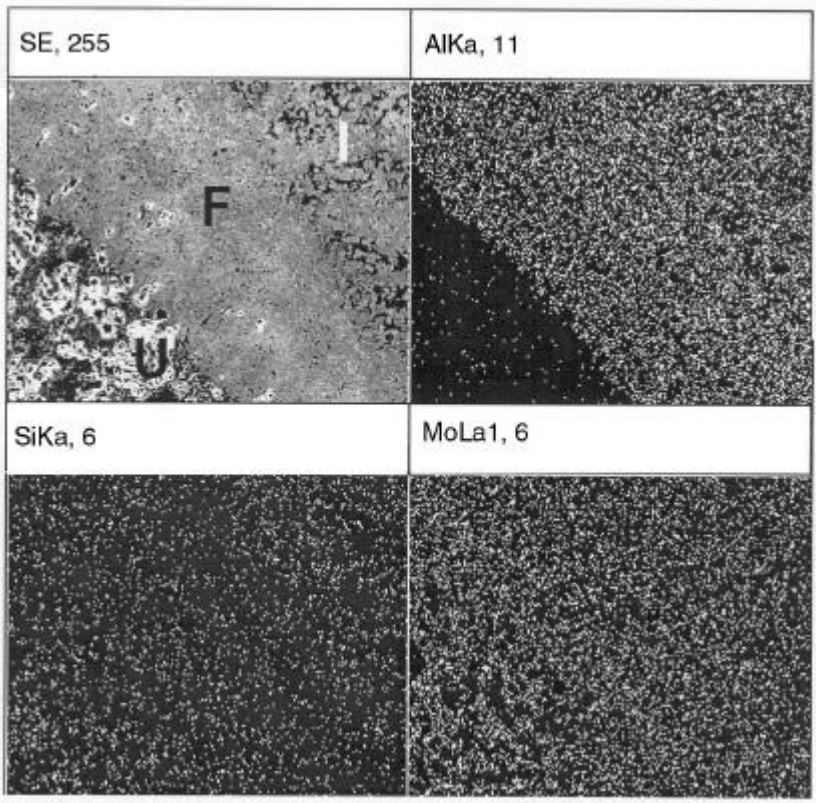

Figure 13. X-ray mapping of infiltrated Mo_5Si_3 at 1400°C for 20 min showing the infiltration front.

Activation energy for the aluminum infiltration into molybdenum silicide preforms was calculated using the Arrhenius equation in the form (reaction rate constant, $K = CL/t$, C being the proportionality constant)

$$CL/t = A \exp [-Ea/RT], \tag{4}$$

where A is the Arrhenius constant, L, t and T are the infiltration length, duration and temperature respectively, and R is the universal gas constant. Time was maintained at 20 min in the first set of experiments. The logarithm of infiltration length (in Mo_5Si_3 preform) as a function of inverse temperature (T) is shown in figure 14. From the slope of the above plot, activation energy (E_a) of the process was found to be ~26 kJ/mol. Activation energy was also calculated for the infiltration of Al into 60% dense Mo_5Si_3 preform. It was found to be ~21 kJ/mol. Following the same procedure, activation energy for the infiltration into $MoSi_2$ preform was calculated as ~300 kJ/mol. In the next set of experiments where temperature was maintained at 1400°C and the duration of infiltration was varied, L vs t is also plotted (for Mo_5Si_3 preform) in figure 14. It is seen that the length of infiltration initially increases linearly with time and then become constant for higher duration. Equation (4) can be rewritten as,

$$\ln L = \ln \frac{At}{C} - \frac{E_a}{RT}. \tag{5}$$

The activation energy calculated from the intercept of ln L vs ln t plot of initial points and using the value of A/C from (4) is ~30 kJ/mol.

The high activation energy for the infiltration of aluminum into $MoSi_2$ preform indicates that chemical reaction and formation of MAS is the rate-determining step. On the other hand, despite being a reactive melt infiltration, the activation energy is very low for the process of infiltration of aluminum into Mo_5Si_3. This means that the infiltration

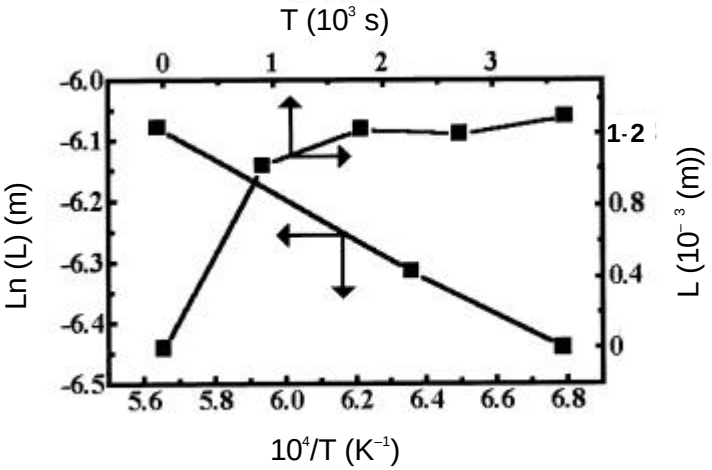

Figure 14. ln(L) vs $1/T$ plot as per (4) and L vs t plot as per (5) for the RMI of Al into Mo_5Si_3 preform.

process is mainly governed by the viscous flow of aluminum. Mo that comes out after reaction (3), retards the viscous flow of aluminium, and in turn reduces the infiltration rate. That is the reason why the activation energy is 26 kJ/mol, three times more than the activation energy for the viscous flow of aluminum (8·4 kJ/mol). Again, lowering of activation energy with lowering of preform density proves the fact that infiltration is governed by viscous flow mechanism. In the L vs t plot initial increase in the rate is due to decrease in the viscosity of aluminum but after that the increase in the Mo content saturates the infiltration process. Therefore, the presence of Mo_5Si_3 in $MoSi_2$ preform retards the infiltration process.

4. Conclusions

Some of the shortcomings of molybdenum disilicide-based ceramics can be improved by reinforcement of both brittle and ductile phases. For low temperature oxidation, the 'pest'ing can be controlled by compacting the components to full density. The wear resistance properties show that an *in situ* tribofilm is formed on the surface of the ceramic pin. This film contains the oxides of both the disc and the pin material. On reinforcing with 20 wt% TiB_2, the wear properties improve tremendously. $Mo(Al_x,Si_{1-x})_2$, a related material, has better low temperature toughness. However, synthesizing single phase $Mo(Al_x,Si_{1-x})_2$ by the powder metallurgy route is difficult. Mo_5Si_3 is invariably present as impurity, which deteriorates the oxidation resistance of the components. Hence the melt infiltration technique is used to synthesize composites of $Mo(Al_x,Si_{1-x})_2$. Different preform compositions are attempted for the infiltration. Irrespective of initial composition of the preform the final product is always a composite of $Mo(Al_x,Si_{1-x})_2$ and Al; the value of x is dependent on the preform composition. When the preform is $MoSi_2$, x is found to be 0·25 whereas it is 0·4 when the preform is Mo_5Si_3. Activation energy for the infiltration into $MoSi_2$ preform is ~300 kJ/mol while into Mo_5Si_3 preform it is ~26 kJ/mol. Lower activation energy indicates that infiltration into Mo_5Si_3 preform is mainly governed by the viscous flow of aluminum and in $MoSi_2$ there is a combination of chemical reaction and diffusion.

Acknowledgement

The authors would like to thank NAL management for encouragement. We thank Professor S K Biswas, Indian Institute of Science (IISc), Bangalore for all the help rendered with the wear-resistance experiments. We would also like to thank Dr T A Bhaskaran, NAL and Mr K R Kannan, IISc for taking SEM micrographs. PST and AKB thank the Council of Scientific and Industrial Research, New Delhi and SKR thanks the University Grants Commission, New Delhi for fellowships.

References

1. Meschter P J and Schwartz D S 1989 *J. Met.* **41** 52
2. Nakamura M, Matsumoto S and Hirano T 1990 *J. Mater. Sci.* **25** 3309
3. Petrovic J J and Vasudevan A K 1999 *Mater. Sci. Eng.* **A261** 1
4. Vasudevan A K and Petrovic J J 1992 *Mater. Sci. Eng.* **A155** 1
5. Schlichting J 1978 *High Temp. High Pressures* **10** 241
6. Cook J, Khan A, Lee E and Mahapatra R 1992 *Mater. Sci. Eng.* **A155** 183
7. Jeng Y L and Lavernia E J 1994 *J. Mater. Sci.* **29** 2557

8. Costa e Silva A and Kaufman M J 1993 *Scr. Metall. Mater*. **29** 1141
9. Castro R G, Smith R W, Rollett A D and Stanik P W 1992 *Scr. Metall. Mater*. **26** 207
10. Sadananda K, Feng C R, Mitra R and Deevi S C 1999 *Mater. Sci. Eng.* **A261** 223
11. Xiao L and Abbashian R 1992 *Mater. Sci. Eng*. **A155** 135
12. Alman D E, Shaw K G, Stoloff N S and Rajan K 1992 *Mater. Sci. Eng.* **A155** 85
13. Shaw L and Abbaschian R 1995 *J. Mater. Sci.* **30** 849
14. Stoloff N S and Broglio M 1997 *Scr. Metall. Mater.* **37** 59
15. Mitra R, Eswaraprasad N and Mahajan Y R 1996 *Proc. of Technical Session, 59th Annu. Session Indian Ceram. Soc.*, Anna University, Chennai, p. 474
16. Lawrynowicz D E, Wolfenstine J, Nutt S, Lavernia E J, Bailey D E and Sickinger A 1994 *Mater. Res. Soc. Symp. Proc*. **322** 139
17. Petrovic J J and Honnell R E 1990 *J. Mater. Sci*. **25** 4453
18. Maloney M J and Hecht R J 1992 *Mater. Sci. Eng*. **A155** 19
19. Sadananda K and Feng C R 1995 *Ceram. Eng. Sci. Proc.* **16** 155
20. Petrovic J J and Honnell R E 1990 *Ceram. Eng. Sci. Proc*. **11** 7
21. Hawk J A, Alman D E and Stoloff N S 1994 *Scr. Metall. Mater*. **31** 473
22. Hawk J A, Alman D E and Stoloff N S 1995 *Scr. Metall. Mater.* **32** 725
23. Alman D E, Hawk J A and Petrovic J J 1995 *Scr. Metall. Mater*. **31** 1765
24. Mitra R, Rama Rao V V and Rao A V 1999 *Intermetallics* **7** 213
25. Berztiss D A, Cerchiara R R, Gulbransen E A, Pettit F S and Meier G H 1992 *Mater. Sci. Eng.* **A155** 165
26. Hebsur M G 1994 *Mater. Res. Soc. Symp. Proc.* **350** 177
27. Chou T C and Nieh T G 1994 *Mater. Res. Soc. Symp. Proc*. **288** 965
28. Chou T C and Nieh T G 1993 *J. Mater. Res.* **8** 214
29. Ramasesha S K and Shobu K 1999 *Bull. Mater. Sci*. **22** 769
30. Maruyama T and Yanagihara K 1997 *Mater. Sci. Eng*. **A239** 828
31. Westbrook J H and Wood D L 1964 *J. Nucl. Mater*. **12** 208
32. Ramasesha S K, Tantri S P, Jayasingh M E and Biswas S K 2000 *Trobol. Lett.* **8** 219
33. Jayasingh M E, Tantri S P, Bhaskaran T E, Biswas S K and Ramasesha S K 2001 *Mater. Lett.* (in press)
34. Ramasesha S K, Srikari Tantri P and Bhattacharya A K 2000 *Met. Mater. Process.* **12** 181
35. Tantri S P, Jayasingh M E, Biswas S K and Ramasesha S K 2001 *Mater. Sci. Eng.* (in press)
36. Bhattacharya A K and Ramasesha S K 2001 *Ceram. Int.* **27**, 829
37. Ramasesha S K and Shobu K 1998 *J. Am. Ceram. Soc.* **81** 730
38. Aghajanian M K, Rocazella M A, Burke J T and Keck S D 1991 *J. Mater. Sci*. **29** 447
39. Hillig B 1987 *Ceram. Eng. Sci. Proc.* **8** 834
40. Semlak K A and Rhines F N 1958 *Trans. Metall. Soc. AMIE* **212** 325
41. Kurilko A A, Kurshev G A, Rudyukand V A and Naidich Y V 1984 *Poroshk. Metall. (Engl. Transl.)* **9** 35
42. Zhang G J, Yue X M and Watanabe T 1999 *Key Eng. Mater*. **161** 271
43. Bhattacharya A K, Bhaskaran T A and Ramasesha S K *J. Am. Ceram. Soc.* (in press)